Thermal decoherence of superradiance in lead halide perovskite nanocrystal superlattices

Francesco Mattiotti,[*,†,‡,¶] Masaru Kuno,[†,§] Fausto Borgonovi,[‡,¶] Boldizsár Jankó,[†] and G. Luca Celardo[‖]

†*Department of Physics, University of Notre Dame, Notre Dame, IN, USA*
‡*Dipartimento di Matematica e Fisica and Interdisciplinary Laboratories for Advanced Materials Physics, Università Cattolica del Sacro Cuore, Brescia, Italy*
¶*Istituto Nazionale di Fisica Nucleare, Sezione di Pavia, Pavia, Italy*
§*Department of Chemistry and Biochemistry, University of Notre Dame, Notre Dame, IN, USA*
‖*Benemérita Universidad Autónoma de Puebla, Instituto de Física, Puebla, Mexico*

E-mail: fmattiot@nd.edu

Abstract

Recent experiments by Rainò et al.[1] have documented cooperative emission from $CsPbBr_3$ nanocrystal superlattices, exhibiting the hallmarks of low temperature superradiance. In particular, the optical response is coherent and the radiative decay rate is increased by a factor of three, relative to that of individual nanocrystals. However, the increase is six orders of magnitude smaller than what is theoretically expected from the superradiance of large assemblies, consisting of 10^6 to 10^8 interacting nanocrystals. Here we develop a theoretical model of superradiance for such systems and show that thermal decoherence is largely responsible for the drastic reduction of the radiative decay rate in nanocrystal superlattices. Our theoretical approach explains the experimental results[1] and provides insight into the design of small nanocrystal superlattices, able to show a four orders of magnitude enhancement in superradiant response. These quantitative predictions pave the path towards observing superradiance at higher temperatures.

Keywords

Cooperative effects, superradiance, superfluorescence, quantum materials, quantum dots, $CsPbBr_3$, perovskite, nanocrystals, superlattice

Spontaneous emission is a basic quantum mechanical effect due to the coupling of an excited electronic state with the vacuum state of the electromagnetic field. In an ensemble of identical emitters, cooperative radiation emerges. Called superfluorescence,[2] or superradiance (SR) by Dicke, who first proposed the phenomenon in 1954,[3] this effect arises from the excitation of an ensemble of individual dipole emitters and results in an emissive, macroscopic quantum state. SR has been observed in a variety of systems,[4] with some of the most recent examples being cold atomic clouds,[5] photosynthetic antenna complexes,[6] molecular aggregates,[7,8] quantum dots[9,10] and nitrogen vacancies in nanodiamonds.[11] This effect is relevant in enhancing absorption and energy transfer, which has been proposed to improve the efficiency of light-harvesting systems.[12–16] SR also leads to spectrally ultranarrow laser beams.[17]

In an exciting new development, SR-like behavior has recently been observed at low temperature ($T = 6$ K) in a solid state superlattice of $CsPbBr_3$ perovskite nanocrystals (NCs).[1] These superlattices consist of $\sim 10^6 - 10^8$ individual cubic NCs self-assembled into ordered cubic arrays with dimensions on the order of microns. Lead halide perovskite NC superlattices distinguish themselves from analogous semiconductor NC superlattices[18,19] in that $CsPbBr_3$ NCs have very high emission quantum yields and very short radiative lifetimes.[20] This high sensitivity to incoming photons makes $CsPbBr_3$ NCs ideal candidates for building photon sensors and quantum devices. For this reason, recent experimental evidence of SR in $CsPbBr_3$ NC superlattices[1] represents an exciting development.

Apparent $CsPbBr_3$ NC superlattice SR distinguishes itself from the normal band edge emission of $CsPbBr_3$ NCs in that it exhibits a 2.7 times faster radiative lifetime. Most importantly, the emission is coherent as seen through first- and second-order correlation measurements.

Despite these highly suggestive results, there are notable discrepancies in the experimental observations[1] from what is expected of SR behavior. Our primary concern is the reported 2.7 times radiative rate enhancement. This is because SR radiative rate enhancements scale as N, the number of interacting dipoles.[2,4,21] Given that there are approximately $N \sim 10^6 - 10^8$ NC emitters in the superlattice, the observed factor of 2.7 enhancement easily differs by six orders of magnitude from what is expected at low temperature (6 K). For instance, at similar temperatures, SR enhancement in molecular systems is hundreds of times larger.[7,8]

We have now developed an open quantum model,[24] based on the use of well-known non-Hermitian radiative Hamiltonians,[25] to rationalize SR-like emission from NC superlattices in the weak excitation regime. Our model specifically applies to the low fluence (500 nJ cm^{-2}) fluorescence measurements of Ref. 1 (see **Supporting Information, section S1**). This regime is also relevant for renewable energy applications, involving light harvesting, and has previously been invoked when modeling the SR of molecular aggregates[25] and cold atom gases.[22,26]

We model the $CsPbBr_3$ NC band edge electronic structure using a four-level system, which accounts for the main isotropic $s - p$ transitions of single NCs.[20] In the low fluence regime, we limit our considerations to the single excitation manifold, spanned by the states $|n, \alpha\rangle = \hat{a}^\dagger_{n,\alpha} |G\rangle$, where one excitation is present on the $\alpha = x, y, z$ state of the nth NC, while all the other NCs are in their ground states. Here, $|G\rangle$ is the ground state of the whole system, where no excitation is present, and $\hat{a}^\dagger_{n,\alpha}$ is an operator that creates an excitation on the αth state of the nth NC. The label $\alpha = x, y, z$ denotes the three angular momentum states of the p orbital. In our simulations, we consider an ensemble of N NCs, each of edge length l, forming a cubic superlattice of edge length $L \gg l$. The center-to-center distance between neighboring NCs is $l' = l + b$, which accounts for the presence of surface ligands. In our simulations, $b = 1$ nm, as commonly seen in superlattices.[27]

The following $3N \times 3N$ non-Hermitian, radiative Hamiltonian

$$\hat{H} = \sum_{n=1}^{N} \sum_{\alpha=x,y,z} E_n |n, \alpha\rangle \langle n, \alpha| + \sum_{\alpha,\beta} \sum_{n \neq m} J^{\alpha\beta}_{mn} |m, \alpha\rangle \langle n, \beta| \quad (1a)$$

accounts for interactions between individual NCs and their common light field[22,25] where point-dipole couplings have been implicitly assumed (see **Supporting Information, section S2**). Furthermore, $E_n = \hbar\left(\omega_0 - i\frac{\gamma_r}{2}\right)$ is the complex self-energy of the nth NC, where $\hbar\omega_0 = 2.38$ eV is the NC transition energy[1] and $\gamma_r = \mu^2\omega_0^3\sqrt{\epsilon_r}/(3\pi\epsilon_0\hbar c^3) = 2.5$ ns^{-1} is the radiative decay rate of a single NC[1] (with $\mu = 23$ D being the single NC transition dipole moment, $\epsilon_r = 4.8$ the relative dielectric permittivity at frequency ω_0,[20] ϵ_0 the vacuum permittivity and c the speed of light). Moreover, $J^{\alpha\beta}_{mn} = \Omega^{\alpha\beta}_{mn} - \frac{i}{2}\Gamma^{\alpha\beta}_{mn}$ with the real and imaginary

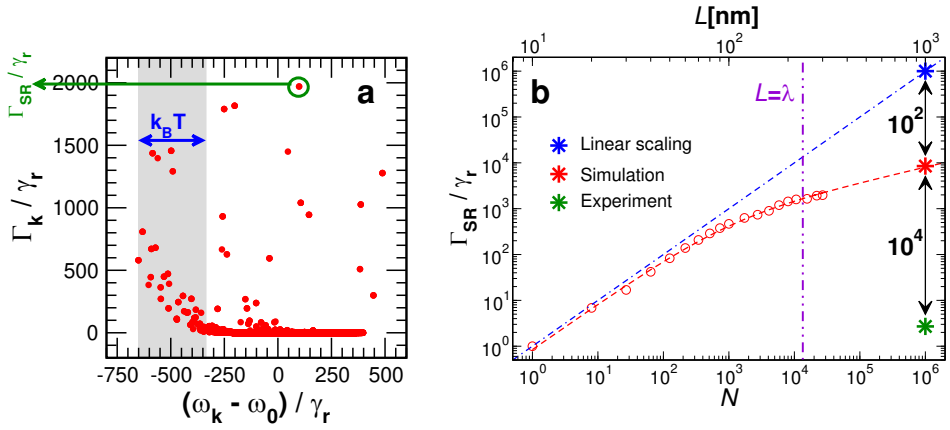

Figure 1: **a** Eigenvalues in the complex plane of the Hamiltonian $\hat{H}$ (see Eq. (1a)) for a cubic superlattice of $N = 30^3$ NCs. $\hat{H}$ has dimensions $3N \times 3N = 6.561 \times 10^9$. The SR rate, Γ_{SR}, corresponding to the maximal decay rate, is circled green. The grayed region denotes the energy range within k_BT of the ground state energy at $T = 6$ K. **b** Plot of Γ_{SR}/γ_r versus N. The dashed blue line represents the maximal SR rate theoretically achievable. The violet vertical dash-dotted line indicates where L equals the wavelength λ of emitted light within the material. Simulation data (circles) have been fit (dashed red line) to the function $\Gamma_{SR}/\gamma_r = CN/(N^{2/3} + N_{cr}^{2/3})$ (fit parameters: $C = 81.2$ and $N_{cr} = 932$), that interpolates between the $\sim N$ behavior (expected for $L \ll \lambda$) and $\sim N^{1/3}$ (expected for $L \gtrsim \lambda$).[22,23] The green symbol marks the experimental results of Ref. 1. Parameters for **a**,**b**: single NC radiative lifetime $1/\gamma_r = \tau_r = 0.4$ ns, single NC band edge energy $\hbar\omega_0 = 2.38$ eV, relative dielectric constant at optical frequencies $\epsilon_r = 4.8$ and NC edge length, $l = 9$ nm.

parts given by

$$\Omega_{mn}^{\alpha\beta} = \frac{\hbar\gamma_r}{2}\Big\{ y_0(k_0 r_{mn})\,\hat{e}_\alpha\cdot\hat{e}_\beta - \frac{y_2(k_0 r_{mn})}{2}\left[\hat{e}_\alpha\cdot\hat{e}_\beta - 3(\hat{e}_\alpha\cdot\hat{r}_{mn})(\hat{e}_\beta\cdot\hat{r}_{mn})\right]\Big\}, \tag{1b}$$

$$\Gamma_{mn}^{\alpha\beta} = \hbar\gamma_r\Big\{ j_0(k_0 r_{mn})\,\hat{e}_\alpha\cdot\hat{e}_\beta - \frac{j_2(k_0 r_{mn})}{2}\left[\hat{e}_\alpha\cdot\hat{e}_\beta - 3(\hat{e}_\alpha\cdot\hat{r}_{mn})(\hat{e}_\beta\cdot\hat{r}_{mn})\right]\Big\}. \tag{1c}$$

Here, $y_0(x)$, $y_2(x)$, $j_0(x)$, and $j_2(x)$ are spherical Bessel functions, $k_0 = \omega_0\sqrt{\epsilon_r}/c$ is the transition wavenumber, $\hat{e}_\alpha$ is the unit vector along the α direction, r_{mn} is the distance between the mth and nth NC and $\hat{r}_{mn}$ is the unit vector joining them. $J_{mn}^{\alpha\beta}$ describes the full radiative coupling between different NC transition dipoles in the superlattice.

A similar approach has recently been proposed to model two-dimensional $CsPbBr_3$ NC superlattices.[28] The employed dipolar near-field coupling, however, is not valid for distances larger than λ, the NC band edge transition wavelength inside the material. This means that collective radiation cannot be analyzed for typical experimental system sizes where $L \approx 5\lambda$ (see **Supporting Information, section S1**). Within our approach interference between different emitters is implicitly accounted for by $J_{mn}^{\alpha\beta}$ even for distances larger than λ. Diagonalizing $\hat{H}$, in turn, yields complex eigenenergies $E_k = \hbar\left(\omega_k - i\frac{\Gamma_k}{2}\right)$ where the imaginary part is related to the radiative lifetime $\tau_k = \Gamma_k^{-1}$ of the kth eigenstate.

Figure 1a shows the typical complex spectrum for a superlattice of $N = 30^3 = 27,000$ NCs with individual NC edge lengths of $l = 9$ nm and an associated center-to-center distance of $l' = 10$ nm. Here both the decay widths ($\hbar\Gamma_k$) and the real energies ($\hbar\omega_k$) are normalized with the single NC decay width $\hbar\gamma_r \approx 1.6$ μeV. We identify the SR decay, Γ_{SR}, as the maximal decay rate predicted (cf. circle in **Figure 1a**), since time evolution from a generic initial state is dominated by $\sim \exp(-\Gamma_{SR}t)$, assuming $T = 0$ K (see **Supporting Information, section S3**). Note

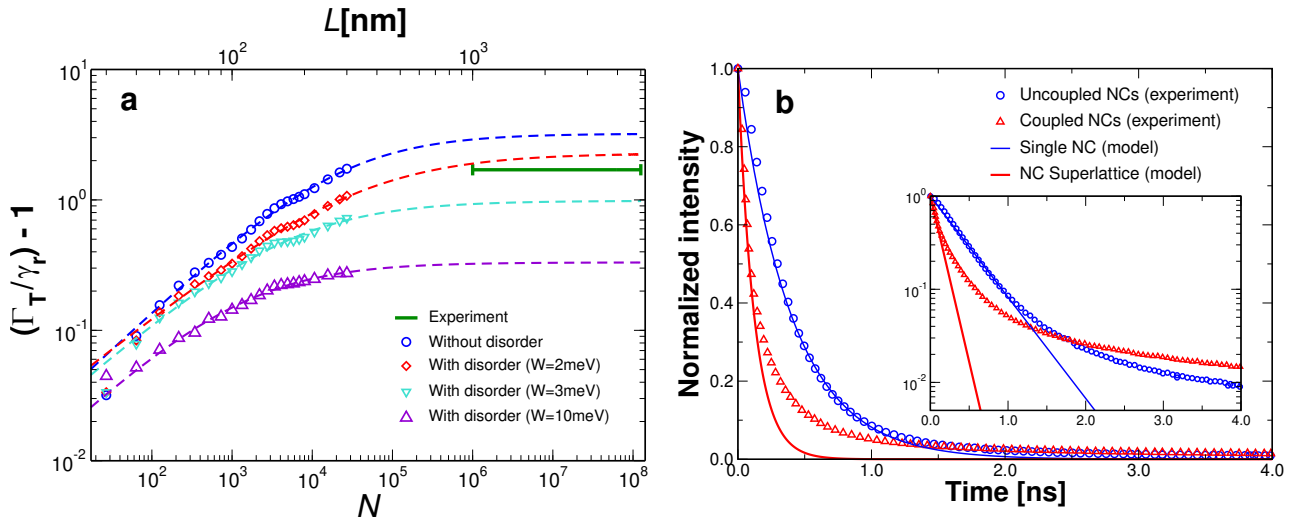

Figure 2: **a** Thermal average of the normalized radiative decay, $(\Gamma_T/\gamma_r) - 1$, (Eq. (2)) versus N. Note that we subtract one from the normalized thermal radiative rate to improve the visibility at small decay rates. The 2.7 enhancement reported in Ref. 1 is shown in solid green. Symbols are obtained from numerical diagonalization of Eq. (1a). Dashed lines are best fits using the function $(\Gamma_T/\gamma_r) - 1 = AN^B/(N^B + N_{sat}^B)$, with fit parameters A, B, N_{sat} (values in **Supporting Information, section S6**). **b** Comparison of the experimental[1] NC superlattice SR radiative decay rate to theory, accounting for thermalization and static disorder ($W = 2$ meV). Temperature is 6 K. "Coupled NCs" refers to the decay of coupled NCs in a superlattice, while "Uncoupled NCs" refers to the measured decay of isolated, non-interacting NCs. Inset: same data on a logarithmic y-scale. In both **a,b**, $\hbar\omega_0 = 2.38$ eV, $\gamma_r = 2.5$ ns^{-1}, $\epsilon_r = 4.8$ and $l = 9$ nm.

that the energy of the maximal SR state is highly dependent on the superlattice geometry, dimension and on the ratio L/λ, see **Supporting information, section S4.**

Given that the system size we consider, $N = 30^3$, is two orders of magnitude smaller than that used experimentally[1] ($N \sim 10^6 - 10^8$), we study how Γ_{SR} scales with N and extrapolate its value to experimentally-relevant superlattice sizes using the well-established relationship:[22,23] $\Gamma_{SR} \propto N$ for $L \ll \lambda$ and $\Gamma_{SR} \propto N/(L/\lambda)^2$ for for $L \gtrsim \lambda$, which implies $\Gamma_{SR} \propto N^{1/3}$ for a fixed NC superlattice density of N/L^3.

By extrapolating Γ_{SR} to large N, our model predicts a SR lifetime of order $\tau_{SR} \sim 0.04$ ps for a NC superlattice of similar size to the one studied experimentally[1] (see **Figure 1b** and **Supporting Information, section S3**). Thus we predict at least $\Gamma_{SR}/\gamma_r \sim 10^4$ for the experimental NC and superlattice size, which is four orders of magnitude larger than the enhancement observed in Ref. 1.

At this point, we suggest that what prevents agreement between theory and experiment is the absence of an explicit consideration of the sensitivity of SR to thermalization-induced coherence losses and structural disorder. Indeed, thermal noise suppresses quantum coherence, especially when k_BT becomes comparable to the spectral width of the interacting ensemble (typically of the same order as the nearest-neighbor coupling J). This can lead to highly suppressed SR in the regime experimentally investigated,[1] since at 6 K $k_BT = 0.5$ meV, which is $\sim$ 3 times larger than the estimated $J = 0.14$ meV coupling between nearest NC neighbors.

We therefore account for thermalization effects on NC superlattice SR by taking thermal averages of all superradiant and subradiant eigenstate emission rates,[29,30] namely

$$\Gamma_T = \frac{1}{Z}\sum_k \Gamma_k e^{-\hbar\omega_k/(k_BT)} \ , \qquad (2)$$

where $Z = \sum_k e^{-\hbar\omega_k/(k_BT)}$ is the partition func-

tion. From Equation (2), a corresponding emission intensity is $I(t) \propto \exp(-\Gamma_T t)$, with Γ_T the thermal decay rate. Thermalization therefore suppresses SR so that $\Gamma_T \approx \gamma_r$ (with $\gamma_r = \tau_r^{-1}$) if $k_B T$ is comparable to the spectral width of the coupled system. Note that in using Equation (2) we implicitly assume that thermal relaxation dominates all other relaxation processes in the material (see details in **Supporting Information, section S5**).

Figure 2a shows that by taking thermal averages for different superlattice sizes (blue circles), we observe an initial fast increase of Γ_T for small N, followed by a slower increase at large N. Assuming saturation in the limit $N \to \infty$ (see **Supporting Information, section S7**), we estimate $\Gamma_T/\gamma_r \approx 4.2$ for $N \sim 10^6 - 10^8$. This is in excellent agreement with the experimental results[1] where $\Gamma_{EXP}/\gamma_r \approx 2.7$.

An even better correspondence is found by taking into account structural disorder in the superlattice, stemming from NC size heterogeneities[1,31] as well as inhomogeneities in NC positions and orientations. To estimate the impact this structural disorder has on SR, we consider excitation energy fluctuations, which we model by adding an on-site disorder of strength W (see also **Supporting Information, section S8**). This form of disorder has previously been used[32] to model the effects of different sources of time-independent disorder in various systems.

By introducing such disorder and extrapolating the results to experimentally-relevant superlattice sizes, we find excellent agreement with experiment[1] for W between 2 meV and 3 meV, see **Figure 2a** where the experimental[1] result is shown in green. Note these values of W are several times larger than the nearest-neighbor coupling $J = 0.14$ meV ($W/J \approx 15$).

Figure 2b now compares the theoretical decay, Γ_T, for $W = 2$ meV (red line) to the experimental emission intensity decay reported in Ref. 1 (red triangles). Our theoretical emission intensity accounts for $\sim 70\%$ of the experimental intensity decay. A discrepancy between theory and experiment is visible at long times (see also inset). This likely reflects omissions in the theory, namely not accounting for non-radiative processes in NCs that lead to non-unity emission quantum yields.[33] This interpretation is confirmed by the non-exponential decay of the emission from an ensemble of uncoupled NCs (blue circles, **Figure 2b**). Modelling such processes is highly non trivial since they should account for dynamical transitions between radiative and non-radiative channels, possibly including activation/deactivation processes for non-radiative channels that induce blinking.[34,35] At this point, however, our proposed theoretical framework, which accounts for thermalization and structural disorder, generally rationalizes the superradiant accelerated PL decay reported in Ref. 1.

In Ref. 1 it was also observed that the emission spectrum of single superlattices consists of several emission peaks, with the SR emission band being redshifted relative to the emission of uncoupled NCs by 64 ± 6 meV (an average across 10 superlattices). This redshift cannot be explained by dipolar couplings between NCs in our model, which at best induces a few meV redshift to the SR emission, see **Supporting Information, section S9.**

While the origin of a redshifted emission from superlattices remains debated,[36–42] (see **Supporting Information, section S9.**), we conjecture here that the SR redshifted emission observed in Ref. 1 arises from the existence of sub-domains, composed of larger NCs, within individual superlattices. In fact, this has already been suggested by the authors of Ref. 1. Supporting this are $CsPbBr_3$ NC size-dependent band energies that change by hundreds of meV when NC edge lengths change from $l = 3$ nm to $l = 12.8$ nm.[31] Consequently, large NC SR-active sub-domains will show a sizable redshift relative to uncoupled and smaller NCs present in the same NC superlattice. It is of note that larger NCs have an inherently higher likelihood of realizing uniform SR-active sub-domains, due to their smaller relative edge length fluctuations,[31] see **Supporting Information, section S9.**

Indeed, assuming that l varies between 8 nm and 12 nm, which is consistent with the size fluctuations reported in Ref. 1, a 50 meV redshift is readily realized between larger NCs and

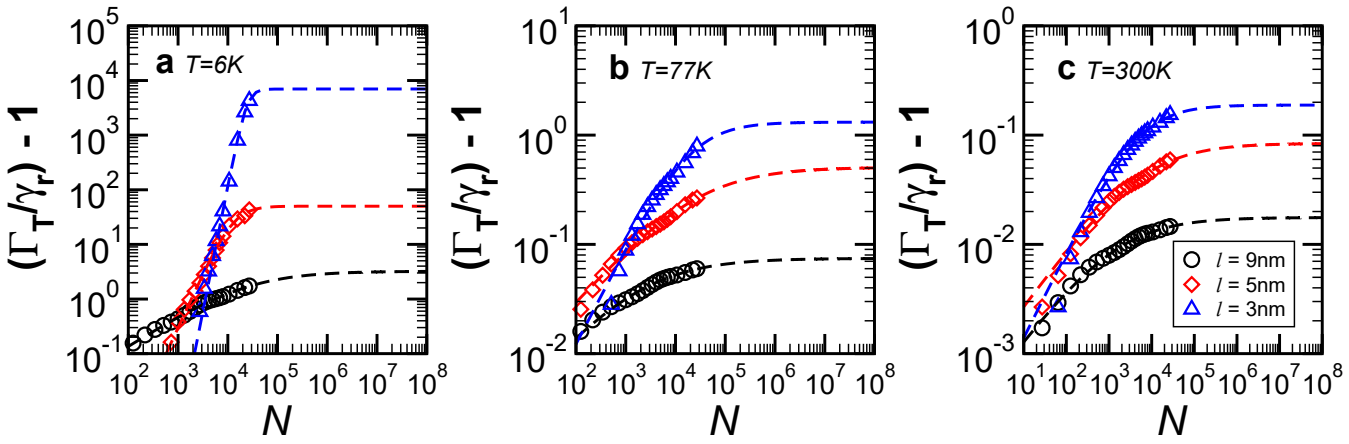

Figure 3: Thermal average of the normalized radiative decay (Eq. (2)) versus N for different temperatures (T = 6 K, 77 K, 300 K). In each panel, the temperature is fixed and each color represents a different NC size (l = 3 nm, 5 nm, 9 nm, see the legend). Dashed lines are best fits with the function $(\Gamma_T/\gamma_r) - 1 = AN^B/(N^B + N_{sat}^B)$, with fit parameters A, B, N_{sat} (values in **Supporting Information, section S6**). In all panels, the excitation energy is $\hbar\omega_0 = 2.38$ eV and the transition dipole moment is $\mu = 23$ D. The relative dielectric constant of NC superlattice effective medium is $\epsilon_r = 4.8$.

their smaller NC counterparts within a given superlattice's residual size distribution (see details in the **Supporting Information, section S9**). The existence of sub-domains made of larger NCs within a superlattice thus rationalize large redshifts of the SR emission.

How large are the sub-domains? In considering this, we note that thermal decoherence, which occurs on the several picoseconds timescale in $CsPbBr_3$ NCs,[43] cannot be neglected when considering their radiative decay, a process that occurs on the hundred picosecond timescale. This ultimately implies that the aforementioned SR sub-domains must be composed of at least $N = 10^4$ NCs to attain a superradiant decay compatible with experiment, see Fig. 2a.

The existence of SR-active sub-domains also explains the large SR linewidth seen in Ref. 1. Namely, Ref. 1 shows SR to have an inhomogeneous linewidth of tens of meV. This exceeds the estimated static disorder in our model by at least an order of magnitude, see Fig. 2a. The discrepancy, however, can be rationalized by the presence of *multiple* SR-active sub-domains within a given superlattice, which is consistent with the presence of substructures in the SR emission band, as noted in Ref. 1. Namely, provided that these sub-domains are composed of NCs with different average edge lengths, inhomogeneous broadening of the experimetal SR will be seen. In whole, the existence SR sub-domains within a given superlattice, where each sub-domain is composed of large NCs, with an average size that differs from sub-domain to sub-domain, self-consistently rationalizes three observations made in Ref. 1: (1) large 64 ± 6 meV redshifts, (2) large 15 ± 4 meV SR inhomogeneous linewidths and (3) SR emission spectral substructure. For more details, see the discussion in **Supporting Information, section S10**.

Finally, our theoretical framework points to ways of enhancing the SR effect in NC superlattices. Specifically, our model suggests that superlattices made of smaller, tightly packed NCs will exhibit stronger couplings, implying enhanced SR decays and better prospects for realizing high temperature SR.

We demonstrate this by decreasing component NC edge lengths, l, below $CsPbBr_3$'s exciton Bohr diameter of 7 nm.[20,31] In what follows, a NC transition dipole moment of $\mu = 23$ D and a radiative decay rate of $\gamma_r = 2.5$ ns^{-1} is assumed since both parameters are weakly size-dependent in the range of NC

sizes explored.[20,31,44] Near-field dipole coupling strengths, in contrast, increase due to smaller inter-NC separations. This stems from nearest-NC neighbor couplings scaling as $J \approx \mu^2/(l')^3$ (see **Supporting Information, section S2**).

We consider NCs as small as $l = 3$ nm, compatible with the current lower bound for size-controlled $CsPbBr_3$ NCs.[31] In the case of $l = 3$ nm, the estimated coupling between NCs is $J \approx 2.1$ meV. This is 15 times larger than that in the $l = 9$ nm NC superlattice studied in Ref. 1.

Figure 3 shows the dependence of Γ_T with NC superlattice size, for superlattices made of $l = 3$ nm and $l = 5$ nm NCs. The $l = 9$ nm case is included for comparison purposes. Each panel in **Figure 3** considers a different temperature ($T = 6$ K, 77 K, 300 K). It is clear that decreasing l enhances the SR effect at all temperatures. The largest enhancement occurs at $T = 6$ K for $l = 3$ nm.

By assuming enhancement saturation at large N, we estimate Γ_T for realistically large superlattices ($N \sim 10^8$) made of $l = 3, 5, 9$ nm NCs. At $T = 6$ K, we predict $\Gamma_T/\gamma_r \approx 4.2$ for $l = 9$ nm, in excellent agreement with experiment.[1] For $l = 5$ nm and $l = 3$ nm, we find $\Gamma_T/\gamma_r \approx 50$ and $\Gamma_T/\gamma_r \approx 7000$ respectively at $T = 6$ K. The latter $l = 3$ nm enhancement is three orders of magnitude larger than that reported in Ref. 1.

The modeling therefore suggests that small NCs can be used to significantly increase the temperature range where it is possible to observe NC superlattice SR. To illustrate this, **Figure 3b** shows that the expected SR decay rate enhancement for a $l = 3$ nm NC superlattice is $\Gamma_T/\gamma_r \approx 2.3$ at liquid nitrogen temperature ($T = 77$ K). This raises exciting prospects for realizing robust NC superlattice SR at significantly higher temperatures than 6 K in the near future.

Before concluding, it is important to consider the role of static disorder for different NCs sizes. Indeed, band edge transition energies vary with size, especially at small l.[31] This, in turn, implies that small NCs will exhibit energy disorder parameters larger than those of their larger NC counterparts for identical size distributions. Nevertheless, as shown in **Supporting Information, section S10**, the ratio W/J (where W is the disorder strength and J is the coupling between neighbor NCs) remains almost constant as NC sizes are varied between $l = 3$ nm and $l = 9$ nm. Consequently, since realistic disorder has a minor effect for large NC sizes and for $W/J \approx 15$, we expect a minor effect for small NCs so long as W/J remains of the same order.

In summary, we have developed a theoretical model that explicitly accounts for the effects of thermal decoherence and structural disorder on NC superlattice SR and which rationalizes the SR effect recently observed.[1] Our proposed model also estimates the effects of NC size and temperature on superlattice SR, revealing that superlattices made of smaller, tightly packed NCs will exhibit stronger couplings. Indeed, we predict a SR enhancement of at least three orders of magnitude, using NCs with edge lengths of $l = 3$ nm. This points to the possibility of observing NC superlattice SR at liquid nitrogen temperatures instead of at $T = 6$ K.

We note that our model is generally applicable to other NC assemblies. The only input parameters needed are NC band-edge transition energies, lifetimes, and NC positions within assemblies. Future iterations of the model will account for non-radiative processes in NCs[33] (i.e. non unity emission quantum yields) as well as higher excitation fluences.

Author contributions F.M. and G.L.C. developed the theory. F.M. performed the numerical calculations. All authors contributed to writing the manuscript.

Acknowledgement This research was supported, in part, by the Notre Dame Center for Research Computing through access to key computational resources. F.M. acknowledges support from an international Ph.D. in Science scholarship from the Università Cattolica del Sacro Cuore. F.M. also thanks the University of Notre Dame for its hospitality and the College of Science for its support during the time this work was conducted. M.K. thanks the Division of Materials Sciences and Engineering,

Office of Basic Energy Sciences, U.S. Department of Energy under award DE-SC0014334 for financial support. Partial support from the MURI:MARBLe project under the auspices of the Air Force Office of Scientific Research (award number FA9550-16-1-0362) is acknowledged. M.K. and B.J. also thank the US National Science Foundation (DMR-1952841) for partial financial support. G.L.C. acknowledges the Conacyt project A1-S-22706. We thank Dmitry Baranov for very useful discussions.

Supporting Information Available

Non-Hermitian Hamiltonian for NC superlattices. Point dipole validity. Time-resolved fluorescence at T=0 K without disorder. Geometry dependence of the SR states position. Time-resolved fluorescence with non-zero temperature. Fitting parameters for the saturation function. The saturation assumption. Time-resolved fluorescence at T=0 K with static disorder. Emission redshift. Static disorder and inhomogeneous linewidth.

References

(1) Rainò, G.; Becker, M. A.; Bodnarchuk, M. I.; Mahrt, R. F.; Kovalenko, M. V.; Stöferle, T. Superfluorescence from lead halide perovskite quantum dot superlattices. *Nature* **2018**, *563*, 671–675.

(2) Bonifacio, R.; Lugiato, L. A. Cooperative radiation processes in two-level systems: Superfluorescence. *Phys. Rev. A* **1975**, *11*, 1507–1521.

(3) Dicke, R. H. Coherence in Spontaneous Radiation Processes. *Phys. Rev.* **1954**, *93*, 99–110.

(4) Cong, K.; Zhang, Q.; Wang, Y.; Noe, G. T.; Belyanin, A.; Kono, J. Dicke superradiance in solids [Invited]. *J. Opt. Soc. Am. B* **2016**, *33*, C80–C101.

(5) Araújo, M. O.; Krešić, I.; Kaiser, R.; Guerin, W. Superradiance in a Large and Dilute Cloud of Cold Atoms in the Linear-Optics Regime. *Phys. Rev. Lett.* **2016**, *117*, 073002.

(6) Monshouwer, R.; Abrahamsson, M.; van Mourik, F.; van Grondelle, R. Superradiance and Exciton Delocalization in Bacterial Photosynthetic Light-Harvesting Systems. *The Journal of Physical Chemistry B* **1997**, *101*, 7241–7248.

(7) De Boer, S.; Wiersma, D. A. Dephasing-induced damping of superradiant emission in J-aggregates. *Chemical Physics Letters* **1990**, *165*, 45 – 53.

(8) Fidder, H.; Knoester, J.; Wiersma, D. A. Superradiant emission and optical dephasing in J-aggregates. *Chemical Physics Letters* **1990**, *171*, 529 – 536.

(9) Scheibner, M.; Schmidt, T.; Worschech, L.; Forchel, A.; Bacher, G.; Passow, T.; Hommel, D. Superradiance of quantum dots. *Nature Physics* **2007**, *3*, 106–110.

(10) Brandes, T. Coherent and collective quantum optical effects in mesoscopic systems. *Physics Reports* **2005**, *408*, 315 – 474.

(11) Bradac, C.; Johnsson, M. T.; van Breugel, M.; Baragiola, B. Q.; Martin, R.; Juan, M. L.; Brennen, G. K.; Volz, T. Room-temperature spontaneous superradiance from single diamond nanocrystals. *Nature communications* **2017**, *8*, 1–6.

(12) Higgins, K.; Benjamin, S.; Stace, T.; Milburn, G.; Lovett, B. W.; Gauger, E. Superabsorption of light via quantum engineering. *Nature Communications* **2014**, *5*, 1–7.

(13) Hu, X.; Ritz, T.; Damjanović, A.; Schulten, K. Pigment Organization and Transfer of Electronic Excitation in the Photosynthetic Unit of Purple Bacteria. *the Journal of Physical Chemistry B* **1997**, *101*, 3854–3871.

(14) Strümpfer, J.; Sener, M.; Schulten, K. How quantum coherence assists photosynthetic light-harvesting. *the Journal of Physical Chemistry Letters* **2012**, *3*, 536–542.

(15) Hu, X.; Damjanović, A.; Ritz, T.; Schulten, K. Architecture and mechanism of the light-harvesting apparatus of purple bacteria. *Proceedings of the National Academy of Sciences* **1998**, *95*, 5935–5941.

(16) Şener, M. K.; Olsen, J. D.; Hunter, C. N.; Schulten, K. Atomic-level structural and functional model of a bacterial photosynthetic membrane vesicle. *Proceedings of the National Academy of Sciences* **2007**, *104*, 15723–15728.

(17) Bohnet, J. G.; Chen, Z.; Weiner, J. M.; Meiser, D.; Holland, M. J.; Thompson, J. K. A steady-state superradiant laser with less than one intracavity photon. *Nature* **2012**, *484*, 78–81.

(18) Murray, C. B.; Kagan, C. R.; Bawendi, M. G. Synthesis and Characterization of Monodisperse Nanocrystals and Close-Packed Nanocrystal Assemblies. *Annual Review of Materials Science* **2000**, *30*, 545–610.

(19) Shevchenko, E. V.; Talapin, D. V.; Kotov, N. A.; O'Brien, S.; Murray, C. B. Structural diversity in binary nanoparticle superlattices. *Nature* **2006**, *439*, 55–59.

(20) Becker, M. A.; Vaxenburg, R.; Nedelcu, G.; Sercel, P. C.; Shabaev, A.; Mehl, M. J.; Michopoulos, J. G.; Lambrakos, S. G.; Bernstein, N.; Lyons, J. L., et al. Bright triplet excitons in caesium lead halide perovskites. *Nature* **2018**, *553*, 189–193.

(21) Gross, M.; Haroche, S. Superradiance: An essay on the theory of collective spontaneous emission. *Physics Reports* **1982**, *93*, 301 – 396.

(22) Bellando, L.; Gero, A.; Akkermans, E.; Kaiser, R. Cooperative effects and disorder: A scaling analysis of the spectrum of the effective atomic Hamiltonian. *Phys. Rev. A* **2014**, *90*, 063822.

(23) Guerin, W.; Rouabah, M.; Kaiser, R. Light interacting with atomic ensembles: collective, cooperative and mesoscopic effects. *Journal of Modern Optics* **2017**, *64*, 895–907.

(24) Gullì, M.; Valzelli, A.; Mattiotti, F.; Angeli, M.; Borgonovi, F.; Celardo, G. L. Macroscopic coherence as an emergent property in molecular nanotubes. *New Journal of Physics* **2019**, *21*, 013019.

(25) Grad, J.; Hernandez, G.; Mukamel, S. Radiative decay and energy transfer in molecular aggregates: The role of intermolecular dephasing. *Phys. Rev. A* **1988**, *37*, 3835–3846.

(26) Bettles, R. *Cooperative interactions in lattices of atomic dipoles*; Springer, 2017.

(27) Brennan, M. C.; Toso, S.; Pavlovetc, I. M.; Zhukovskyi, M.; Maras, S.; Kuno, M.; Manna, L.; Baranov, D. Superlattices are greener on the other side: How light transforms self-assembled mixed halide perovskite nanocrystals. *ACS Energy Lett.* **2020**, *5*, 1465–1473.

(28) Vovk, I. A.; Tepliakov, N. V.; Baimuratov, A. S.; Leonov, M. Y.; Baranov, A. V.; Fedorov, A. V.; Rukhlenko, I. D. Excitonic phenomena in perovskite quantum-dot supercrystals. *Phys. Chem. Chem. Phys.* **2018**, *20*, 25023–25030.

(29) Spano, F. C.; Kuklinski, J. R.; Mukamel, S. Temperature-dependent superradiant decay of excitons in small aggregates. *Phys. Rev. Lett.* **1990**, *65*, 211–214.

(30) Meier, T.; Zhao, Y.; Chernyak, V.; Mukamel, S. Polarons, localization, and excitonic coherence in superradiance of biological antenna complexes. *The Journal*

of Chemical Physics **1997**, *107*, 3876–3893.

(31) Brennan, M. C.; Herr, J. E.; Nguyen-Beck, T. S.; Zinna, J.; Draguta, S.; Rouvimov, S.; Parkhill, J.; Kuno, M. Origin of the Size-Dependent Stokes Shift in CsPbBr3 Perovskite Nanocrystals. *Journal of the American Chemical Society* **2017**, *139*, 12201–12208, PMID: 28772067.

(32) Celardo, G. L.; Giusteri, G. G.; Borgonovi, F. Cooperative robustness to static disorder: Superradiance and localization in a nanoscale ring to model light-harvesting systems found in nature. *Phys. Rev. B* **2014**, *90*, 075113.

(33) Frantsuzov, P.; Kuno, M.; Janko, B.; Marcus, R. A. Universal emission intermittency in quantum dots, nanorods and nanowires. *Nature Physics* **2008**, *4*, 519–522.

(34) Frantsuzov, P. A.; Volkán-Kacsó, S.; Jankó, B. Model of Fluorescence Intermittency of Single Colloidal Semiconductor Quantum Dots Using Multiple Recombination Centers. *Phys. Rev. Lett.* **2009**, *103*, 207402.

(35) Frantsuzov, P. A.; Volkán-Kacsó, S.; Jankó, B. Universality of the Fluorescence Intermittency in Nanoscale Systems: Experiment and Theory. *Nano Letters* **2013**, *13*, 402–408.

(36) Baranov, D.; Toso, S.; Imran, M.; Manna, L. Investigation into the Photoluminescence Red Shift in Cesium Lead Bromide Nanocrystal Superlattices. *The Journal of Physical Chemistry Letters* **2019**, *10*, 655–660.

(37) van der Burgt, J. S.; Geuchies, J. J.; van der Meer, B.; Vanrompay, H.; Zanaga, D.; Zhang, Y.; Albrecht, W.; Petukhov, A. V.; Filion, L.; Bals, S.; Swart, I.; Vanmaekelbergh, D. Cuboidal Supraparticles Self-Assembled from Cubic CsPbBr3 Perovskite Nanocrystals. *The Journal of Physical Chemistry C* **2018**, *122*, 15706–15712.

(38) Nagaoka, Y.; Hills-Kimball, K.; Tan, R.; Li, R.; Wang, Z.; Chen, O. Nanocube Superlattices of Cesium Lead Bromide Perovskites and Pressure-Induced Phase Transformations at Atomic and Mesoscale Levels. *Advanced Materials* **2017**, *29*, 1606666.

(39) Tong, Y.; Yao, E.-P.; Manzi, A.; Bladt, E.; Wang, K.; Döblinger, M.; Bals, S.; Müller-Buschbaum, P.; Urban, A. S.; Polavarapu, L.; Feldmann, J. Spontaneous Self-Assembly of Perovskite Nanocrystals into Electronically Coupled Supercrystals: Toward Filling the Green Gap. *Advanced Materials* **2018**, *30*, 1801117.

(40) Imran, M.; Ijaz, P.; Baranov, D.; Goldoni, L.; Petralanda, U.; Akkerman, Q.; Abdelhady, A. L.; Prato, M.; Bianchini, P.; Infante, I.; Manna, L. Shape-Pure, Nearly Monodispersed CsPbBr3 Nanocubes Prepared Using Secondary Aliphatic Amines. *Nano Letters* **2018**, *18*, 7822–7831.

(41) Kovalenko, M. V.; Bodnarchuk, M. I. Lead halide perovskite nanocrystals: From discovery to self-assembly and applications. *CHIMIA International Journal for Chemistry* **2017**, *71*, 461–470.

(42) Wang, K.-H.; Yang, J.-N.; Ni, Q.-K.; Yao, H.-B.; Yu, S.-H. Metal Halide Perovskite Supercrystals: Gold–Bromide Complex Triggered Assembly of CsPbBr3 Nanocubes. *Langmuir* **2018**, *34*, 595–602.

(43) Brennan, M. C.; Forde, A.; Zhukovskyi, M.; Baublis, A. J.; Morozov, Y. V.; Zhang, S.; Zhang, Z.; Kilin, D. S.; Kuno, M. Universal Size-Dependent Stokes Shifts in Lead Halide Perovskite Nanocrystals. *The Journal of Physical Chemistry Letters* **2020**, *11*, 4937–4944.

(44) Kayanuma, Y. Quantum-size effects of interacting electrons and holes in semiconductor microcrystals with spherical shape. *Phys. Rev. B* **1988**, *38*, 9797–9805.

Graphical TOC Entry